

## *Supporting Information*

### **Impact of Nitrogen Configuration on the Anchoring Mechanism of Platinum Nanoparticles on Carbon Substrates: Synergistic Modification for Hydrogen Revolution in Acidic and Alkaline Media**

Qian Zheng<sup>a,b</sup>, Fengshan Yu<sup>a,b</sup>, Zijun Chen<sup>a,b</sup>, Caifang Cao<sup>c</sup>, Jianzhong Ye<sup>d</sup>, Youbei Zhan<sup>d</sup>, Chunxia Wang<sup>a,b,\*</sup>, Guoyong Huang<sup>a,b,\*</sup>, Shengming Xu<sup>e</sup>

<sup>a</sup> College of New Energy and Materials, China University of Petroleum, Beijing 102249, China

<sup>b</sup> State Key Laboratory of Heavy Oil Processing, China University of Petroleum, Beijing 102249, China

<sup>c</sup> Jiangxi University of Science and Technology, Ganzhou 341000, China

<sup>d</sup> Jiangxi Zili Environmental Protection Technology Co., Ltd, Fuzhou 344113, China

<sup>e</sup> Institute of Nuclear & New Energy Technology, Tsinghua University, Beijing 10084, China

\*Corresponding author Email address: cxwang@cup.edu.cn; huanggy@cup.edu.cn

## Experimental Section

### 1. Chemicals

Zinc nitrate hexahydrate ( $\text{Zn}(\text{NO}_3)_2 \cdot 6\text{H}_2\text{O}$ , A.R., 99.998%), 2-methylimidazole ( $\text{C}_4\text{H}_6\text{N}_2$ , A.R., 98%), methanol ( $\text{CH}_3\text{OH}$ , A.R., 98%), ethanol ( $\text{C}_2\text{H}_5\text{OH}$ , A.R., 99.5%), sulfuric acid ( $\text{H}_2\text{SO}_4$ , A.R., 95-97%), platinum chloride hexahydrate ( $\text{H}_2\text{PtCl}_6 \cdot 6\text{H}_2\text{O}$ , A.R., 99.99%), isopropyl alcohol ( $\text{C}_3\text{H}_7\text{OH}$ , A.R., 99.5%) are all from Shanghai Aladdin Biochemical Technology Co., LTD. Nafion (117, Sigma, 5 wt%), carbon black (117, Sigma, 5 wt%) and sodium hydroxide ( $\text{NaOH}$ , A.R., 99.999%) are used for electro-chemical measurements. Commercial 20 wt% Pt/C is bought from Tanaka Kikinzoku Kogyo (TKK).

### 2. Characterizations

X-ray diffraction (XRD, Haoyuan, China) was used to characterize the phase structure of the samples. The target material was copper, and the acceleration voltage and current were 40 kV and 40 mA, respectively. Scanning electron microscope (SEM, ZEISS JSM-7800F, Germany) was used to observe the morphology of the samples, and 200 kV transmission electron microscope (TEM, FEI Tecnai G2 20, USA) was used to analyze the morphology and microscopic size of the products. The elemental contents were analyzed by inductively coupled plasma-optical emission spectrometer (ICP-OES, Avio™ 200, USA). Raman spectroscopy were collected on a laser Raman Spectrometer (HORIBA HR Evolution, French) with the 532 nm laser source to analyze carbon structures. X-ray photoelectron spectroscopy (XPS, Thermo ESCALAB 250Xi, USA) was used to test the binding energy and chemical states of

the elements of the samples, calibrated with the C 1s peak (284.8 eV) as the standard. The specific surface area and pore size analysis was measured with Brunauer-Emmett-Teller analyzer (BET, Micromeritics ASAP 2460, USA).

### **3. Electrochemical experiments**

Electrochemical measurements were carried out using an electrochemical workstation (Chenhua CHI760, China) with a standard three-electrode cell. The prepared catalysts were used as the working electrode material. Before the preparation of the working electrode, the glassy carbon electrode was polished with 50 nm aluminum oxide powder until the surface of the electrode was mirror-like. Next, the electrode was washed with distilled water and anhydrous ethanol in turn, and then dried and set aside. The 4 mg of catalysts and 4 mg of catalysts carbon black were dispersed in a 1 mL mixed solution consisting of 980  $\mu\text{L}$  of isopropyl alcohol and 20  $\mu\text{L}$  of Nafion (5 wt%) solution to obtain the ink, followed by ultrasonic treatment for 2 hours to homogeneously disperse the catalyst powder. Then 10  $\mu\text{L}$  of ink were evenly dropped on the glass carbon electrode. A glassy carbon electrode (3 mm in diameter) coated with the catalyst was used to prepare the electrocatalyst with a Pt loading capacity of 3.64  $\mu\text{g}\cdot\text{cm}^{-2}$  and 8.80  $\mu\text{g}\cdot\text{cm}^{-2}$  for Pt/NC-900 and commercial 20 wt% Pt/C. In alkaline solution, Hg/HgO was the reference electrode, carbon rod was the counter electrode, electrolyte was 1 M KOH. In acid solution, Ag/AgCl was the reference electrode, carbon rod was the counter electrode, electrolyte was 0.5 M H<sub>2</sub>SO<sub>4</sub>. Cyclic voltammetry (CV) tests were conducted to activate the electrode. Subsequently, linear sweep voltammetry (LSV) was performed at a scan rate of 10 mV s<sup>-1</sup>. Electrochemical

impedance spectroscopy (EIS) was performed at an overpotential of 10 mA cm<sup>-2</sup> with a frequency range of 0.01-100 kHz. LSV was conducted before and after 24 h of CV to test the durability.

All the potentials reported herein are without iR correction, which are given versus reversible hydrogen electrode (RHE), the potential ( $E$ ) was converted to the RHE using the following formula:

$$E_{vs\ RHE} = E_{vs\ Hg/HgO} + 0.0592 \times pH + E^0_{Hg/HgO} \quad (E^0_{Hg/HgO} = 0.098\ V) \quad (4)$$

Turnover frequency (TOF) was calculated assuming that all the Pt sites were active.<sup>1</sup> The equation is

$$TOF = j / (2F \times n) \quad (5)$$

where  $j$  is the current density (A cm<sup>-2</sup>) at a specific overpotential, the number 2 indicating a two-electron hydrogen evolution reaction,  $F$  is Faraday's constant (96485.3 C mol<sup>-1</sup>), and  $n$  represents the moles of Pt on the working electrode, which can be calculated from the mass loading of catalyst on the working electrode.

The TOF (H<sub>2</sub>·s<sup>-1</sup>·site<sup>-1</sup>, or s<sup>-1</sup>) of Pt/NC-900 and Pt/C in 0.5 M H<sub>2</sub>SO<sub>4</sub> were calculated as follows:

For Pt/NC-900, the  $n$  value was calculated based on the hypothesis that all Pt atoms in the Pt/NC-900 can act as active centers and are accessible to the electrolyte. The Pt content in the Pt/NC-900 catalyst was determined using the ICP-OES technique. The moles of Pt on the working electrode for Pt/ NC-900 is,

$$n = 5.154 \times 10^{-5} \text{ g} \cdot \text{cm}^{-2} / 195.08 \text{ g} \cdot \text{mol}^{-1} = 2.642 \times 10^{-7} \text{ mol} \cdot \text{cm}^{-2}$$

At  $\eta = -100$  mV,  $j = -104.088 \text{ A} \cdot \text{cm}^{-2} \cdot 10^{-3}$ , thus,

$$\text{TOF} = 104.088 \times 10^{-3} / 2 F n = 2.04 \text{ s}^{-1}$$

For Pt/C, the n value was calculated based on the hypothesis that all Pt atoms in the Pt/C can act as active centers and are accessible to the electrolyte. The Pt content in the Pt/C catalyst was determined using the ICP-OES technique. The moles of Pt on the working electrode for Pt/C is,

$$n = 1.258 \times 10^{-4} \text{ g} \cdot \text{cm}^{-2} / 195.08 \text{ g} \cdot \text{mol}^{-1} = 6.448 \times 10^{-7} \text{ mol} \cdot \text{cm}^{-2}$$

At  $\eta = -100 \text{ mV}$ ,  $j = -87.608 \text{ A} \cdot \text{cm}^{-2} \cdot 10^{-3}$ , thus,

$$\text{TOF} = 87.608 \times 10^{-3} / 2 F n = 0.70 \text{ s}^{-1}$$

#### 4. Density functional theory (DFT) calculations

First-principles density functional theory (DFT) calculations were conducted using the Vienna Ab initio Simulation Package (VASP) software, employing the projector augmented wave (PAW) method for spin-polarized calculations.<sup>2, 3</sup> To accurately account for the electronic exchange and correlation energies, the Perdew-Burke-Enrzerhof (PBE) parametrization of the generalized gradient approximation (GGA) was utilized. Additionally, the core electrons were described using the PAW pseudopotential. For all computational calculations, a cutoff energy of 500 eV was employed for expanding plane waves. To ensure convergence, a convergence criterion of  $10^{-5}$  eV and an interatomic force criterion of  $0.05 \text{ eV} \cdot \text{\AA}^{-1}$  were applied during optimization of the atomic structure. Spin polarization is also taken into account in all subsequent calculations. To prevent any artificial interactions within the slab models, a vacuum layer with a thickness of 20 Å was implemented along the z direction. The Brillouin zone was sampled using the Monkhorst-Pack method, utilizing a  $1 \times 1 \times 1$  k-

point mesh for the structural calculations.<sup>4-6</sup>

The carbon (C) support is a graphene layer originated from a  $8 \times 8$  supercell of graphite. For the pyridinic nitrogen-doped carbon support (NC), two adjacent carbon atoms were removed, and pyridinic nitrogen (N) atoms were introduced to substitute the carbon atoms surrounding the vacancy. Furthermore, a 26-atom  $\text{Pt}_{26}$  cluster was positioned on the previously mentioned supports. The platinum catalyst was modeled with a Pt (111) surface slab cut from an optimized Pt crystal.<sup>7</sup>

The binding energies between the three supports and the  $\text{Pt}_{26}$  cluster were calculated by the following equation:

$$E_b = E_{\text{Pt}/s} - E_{\text{Pt}} - E_s \quad (1)$$

where  $E_{\text{Pt}/s}$ ,  $E_{\text{Pt}}$ , and  $E_s$  are the total energies of the Pt cluster anchored on the support, the Pt cluster, and the support, respectively.

The Gibbs free energy ( $\Delta G$ ) of the adsorption of hydrogen atom was calculated according to the following equation:

$$\Delta G = \Delta E_H + \Delta E_{\text{ZPE}} - T\Delta S_H \quad (2)$$

where  $\Delta E_H$ ,  $\Delta E_{\text{ZPE}}$ , and  $\Delta S_H$  represent the hydrogen absorption energy, the correction of zero-point energy and the entropy difference between the adsorbed hydrogen atom ( $\text{H}^*$ ) and free  $\text{H}_2$  molecule, respectively.  $T$  is the temperature, which was chosen as 298.15 K.  $\Delta E_H$  was calculated according to the following equation:

$$\Delta E_H = E_{\text{total}} - E_{\text{primitive}} - E_{\text{H}_2}/2 \quad (3)$$

where  $E_{\text{total}}$  is the total energy of the system adsorbed with hydrogen atom,  $E_{\text{primitive}}$  is the total energy of the system without absorbing hydrogen atom, and  $E_{\text{H}_2}$  is the energy

of H<sub>2</sub> molecule.

**Figure and caption**

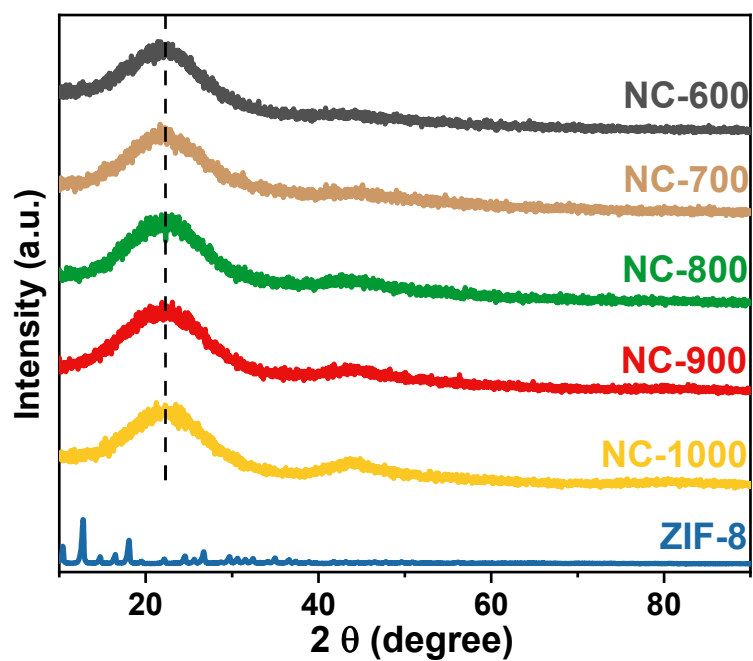


Figure S1. The XRD patterns of NC-x (x=600, 700, 800, 900, 1000).

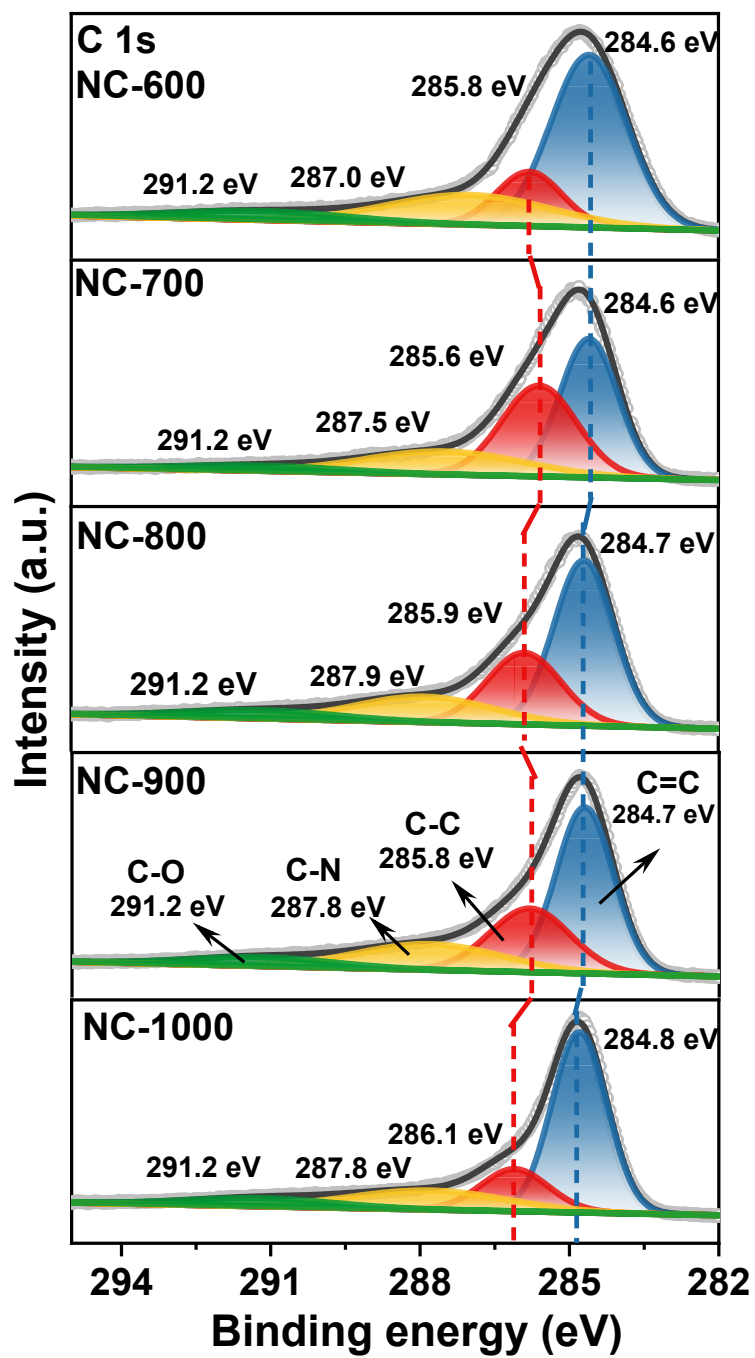


Figure S2. High-resolution XPS spectra C 1s for NC-x (x=600, 700, 800, 900, 1000).

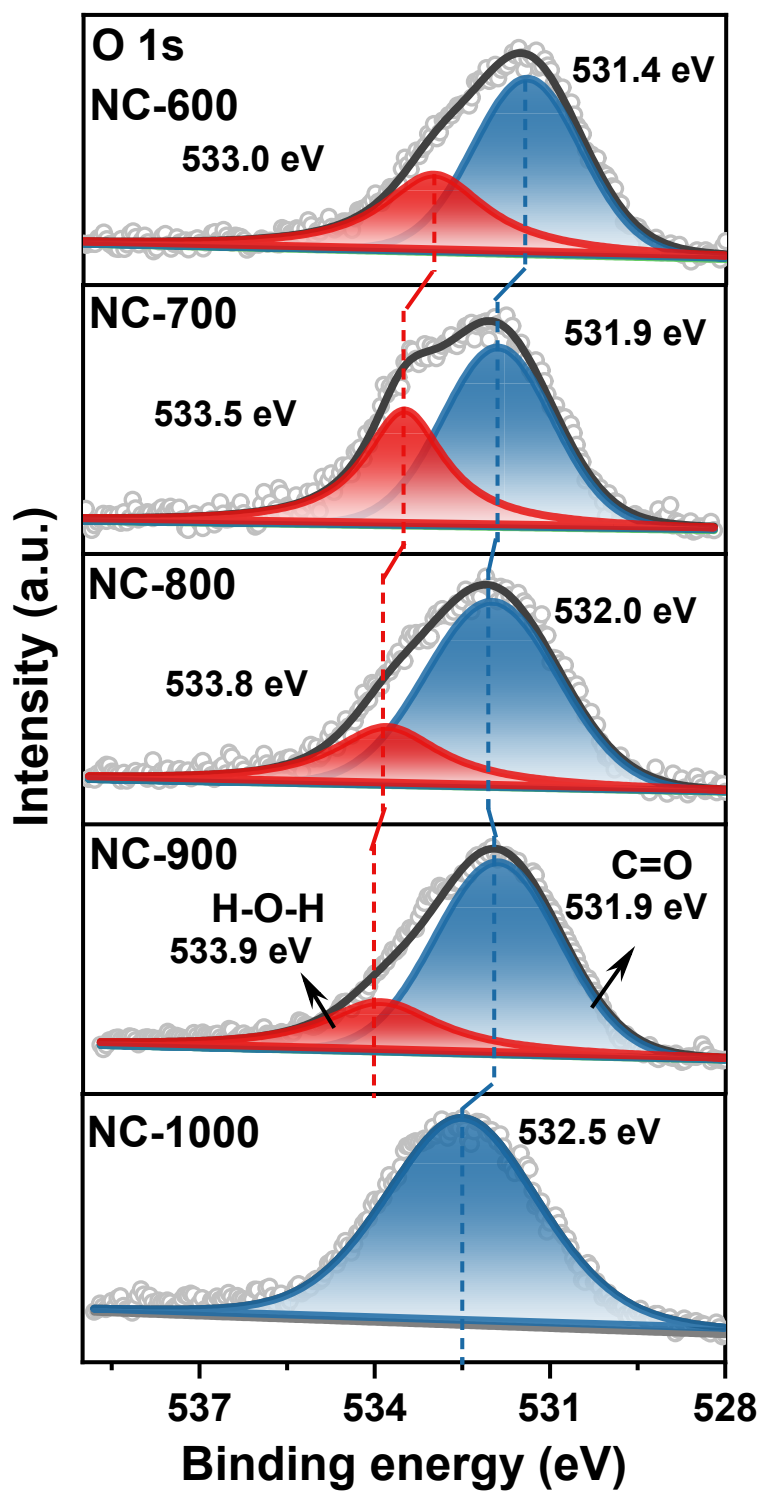


Figure S3. High-resolution XPS spectra O 1s for NC-x (x=600, 700, 800, 900, 1000).

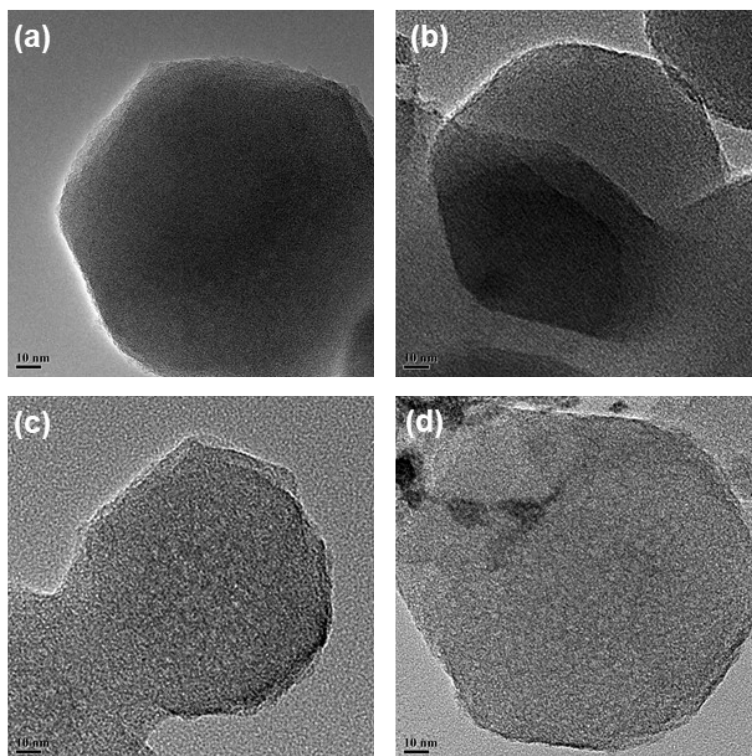


Figure S4. The TEM images of (a) Pt/NC-600, (b) Pt/NC-700, (c) Pt/NC-800, (d) Pt/NC-1000.

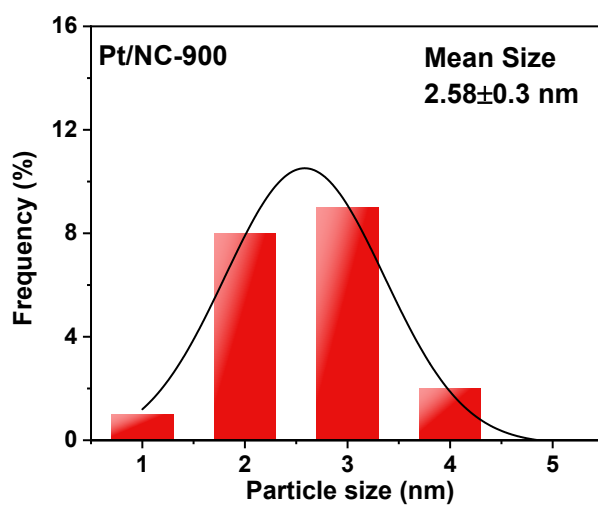


Figure S5. The particle size distribution of Pt/NC-900.

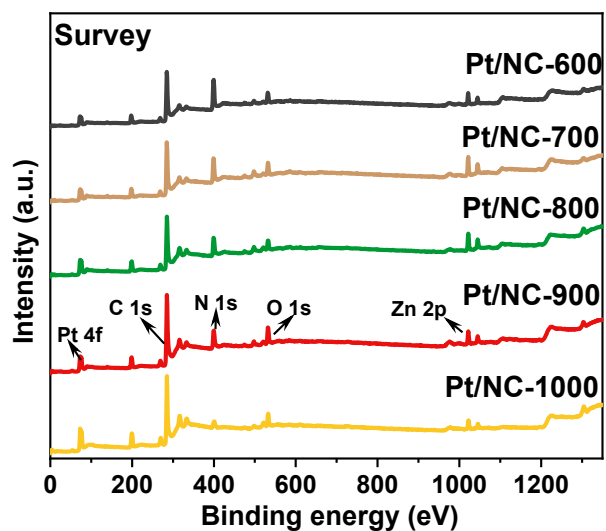


Figure S6. The XPS survey spectra of different Pt/NC-x (x=600, 700, 800, 900, 1000) electrocatalysts.

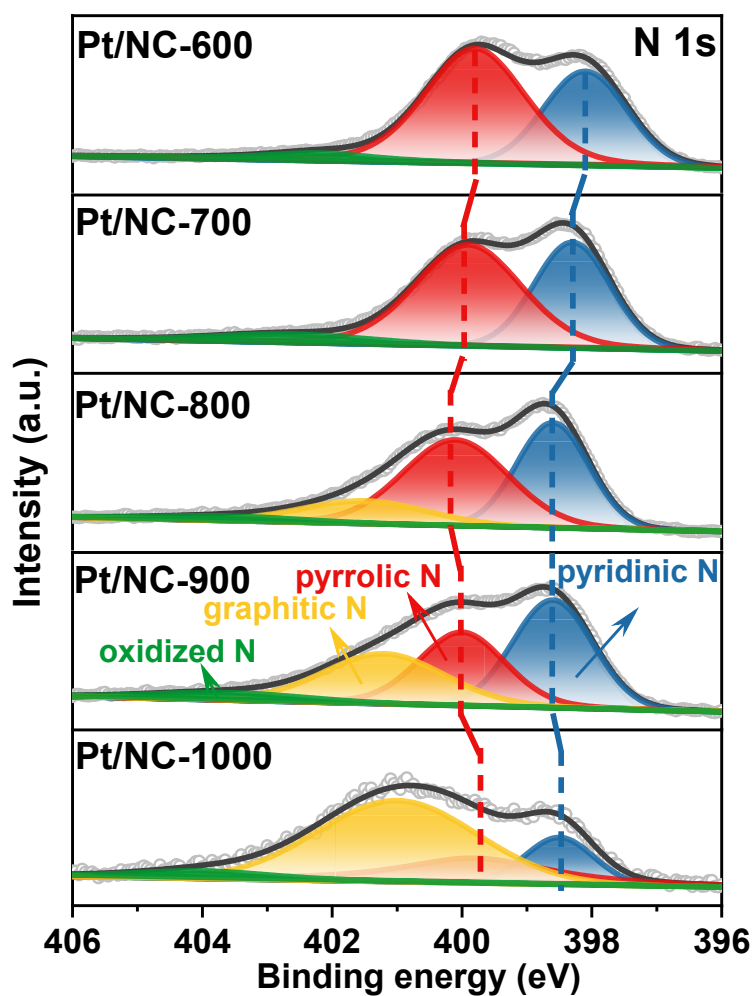


Figure S7. High-resolution XPS spectra N 1s for Pt/NC-x (x=600, 700, 800, 900, 1000).

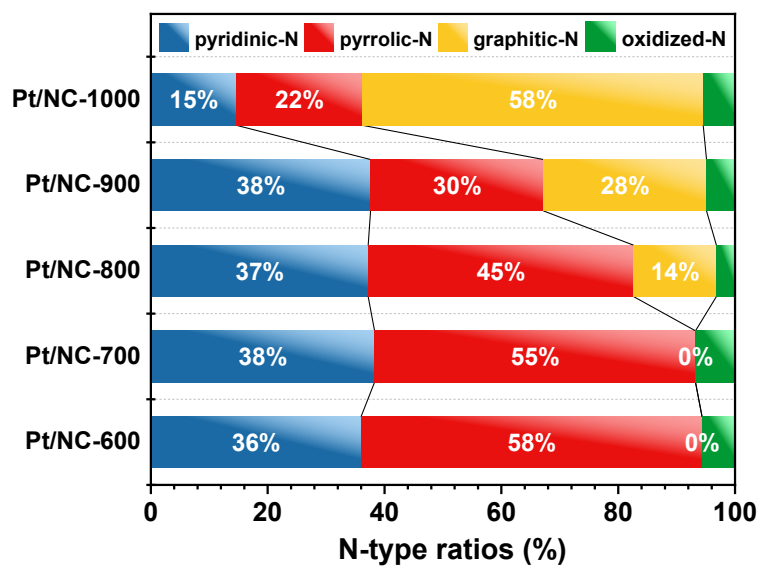


Figure S8. The relative ratios of the different nitrogen species from the N 1s for Pt/NC-x (x=600, 700, 800, 900, 1000 °C).

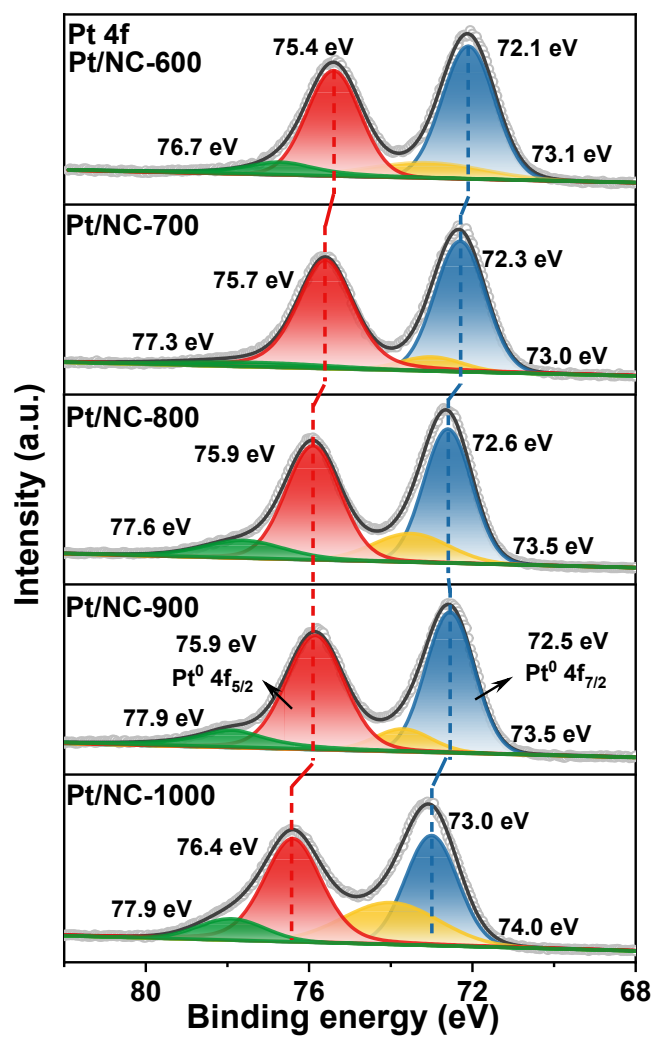


Figure S9. High-resolution XPS spectra of Pt 4f for Pt/NC-x (x=600, 700, 800, 900, 1000).

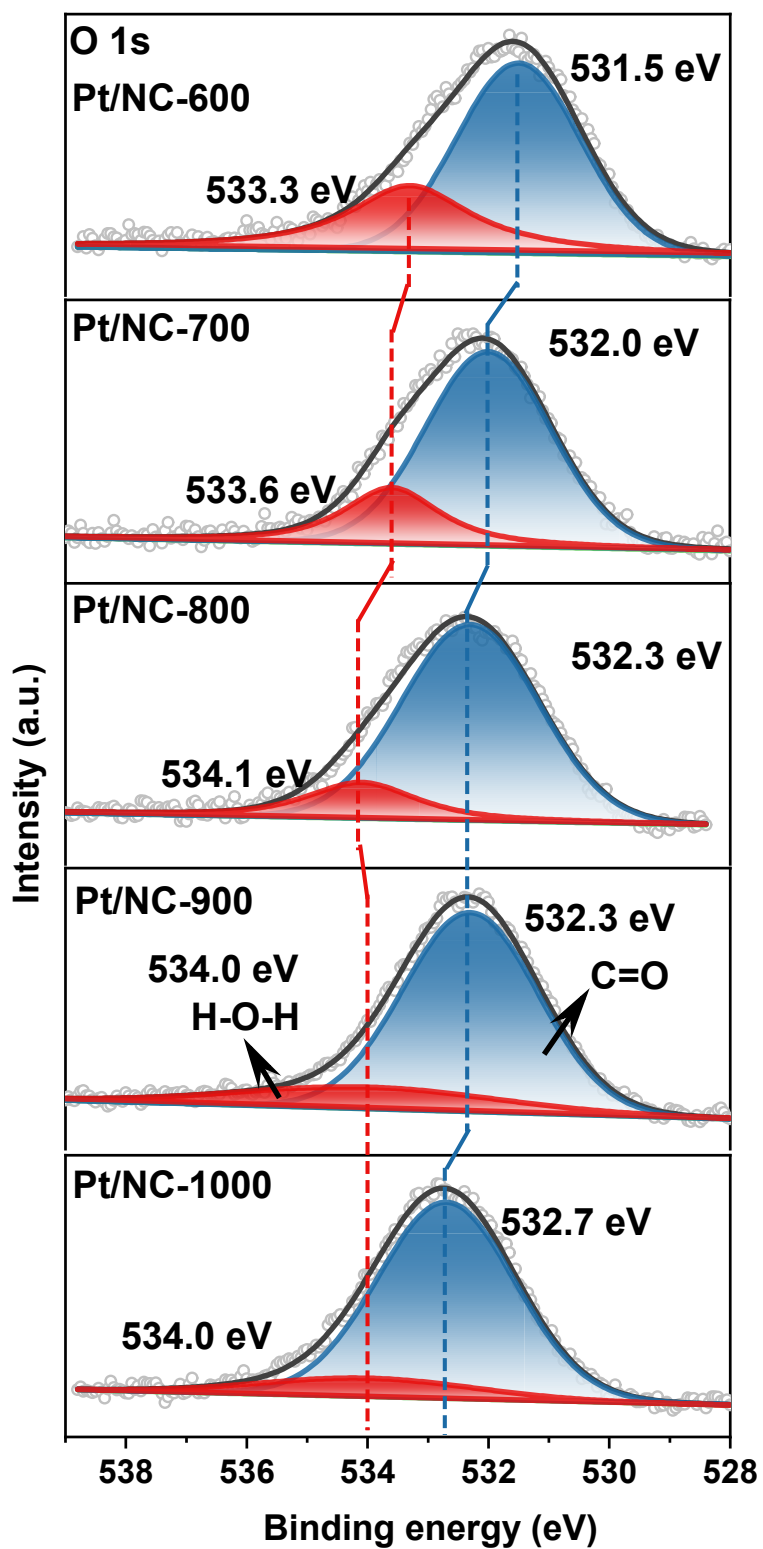


Figure S10. High-resolution XPS spectra O 1s for Pt/NC-x (x=600, 700, 800, 900, 1000).

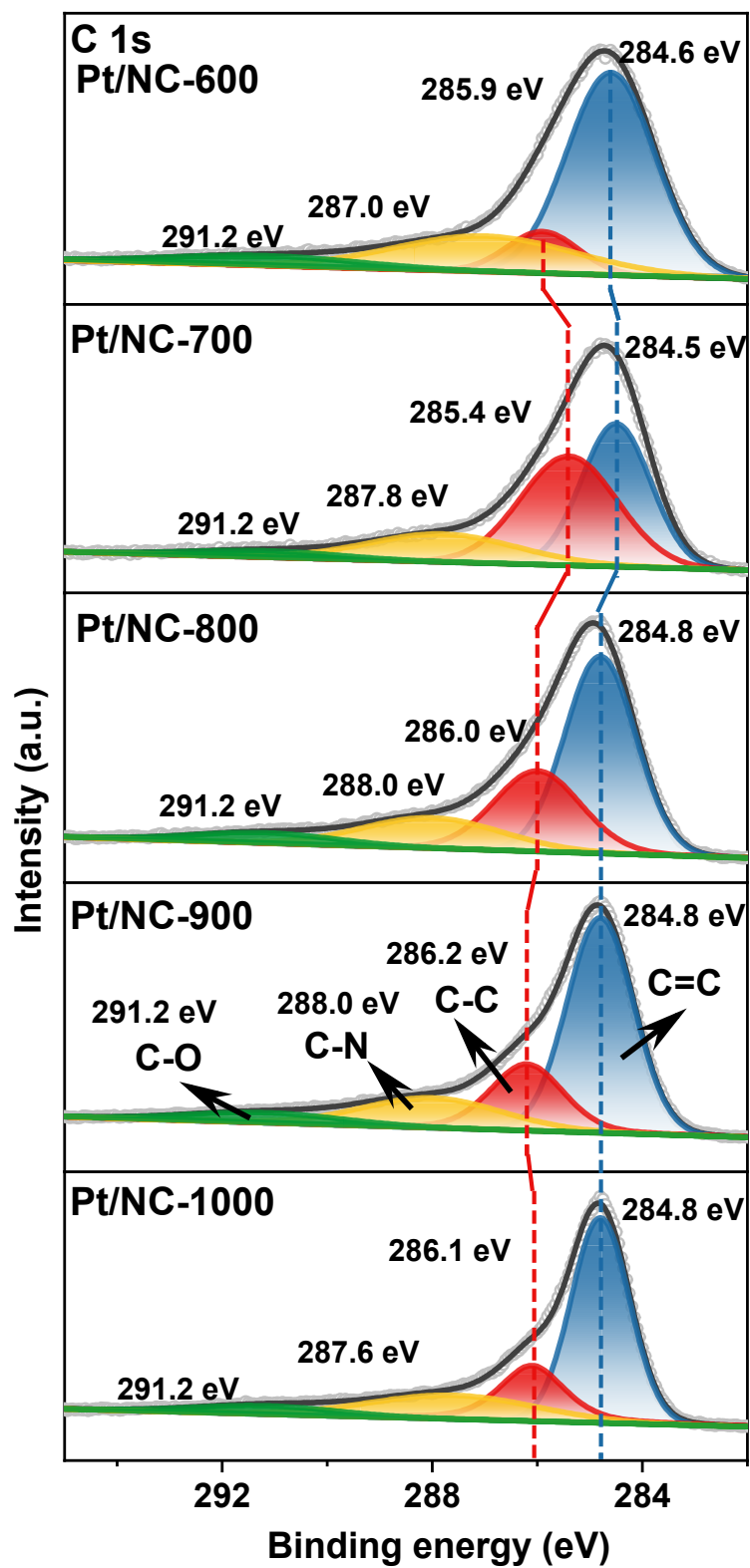


Figure S11. High-resolution XPS spectra C 1s for Pt/NC-x (x=600, 700, 800, 900, 1000).

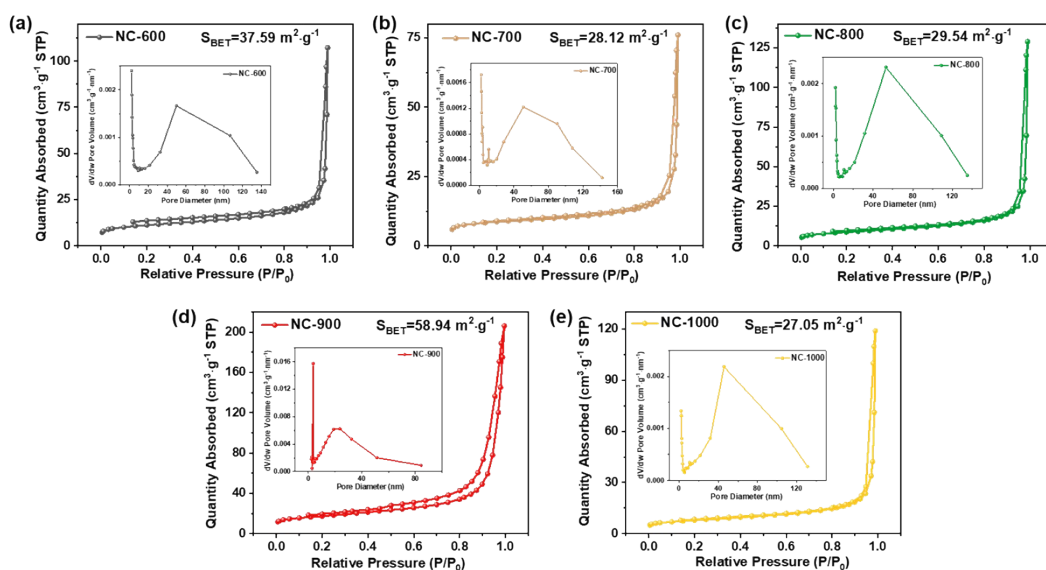


Figure S12. (a-e) N<sub>2</sub> adsorption-desorption isotherm curves and corresponding pore volumes distribution (insets) of the NC-x (x=600, 700, 800, 900, 1000) electrocatalysts.

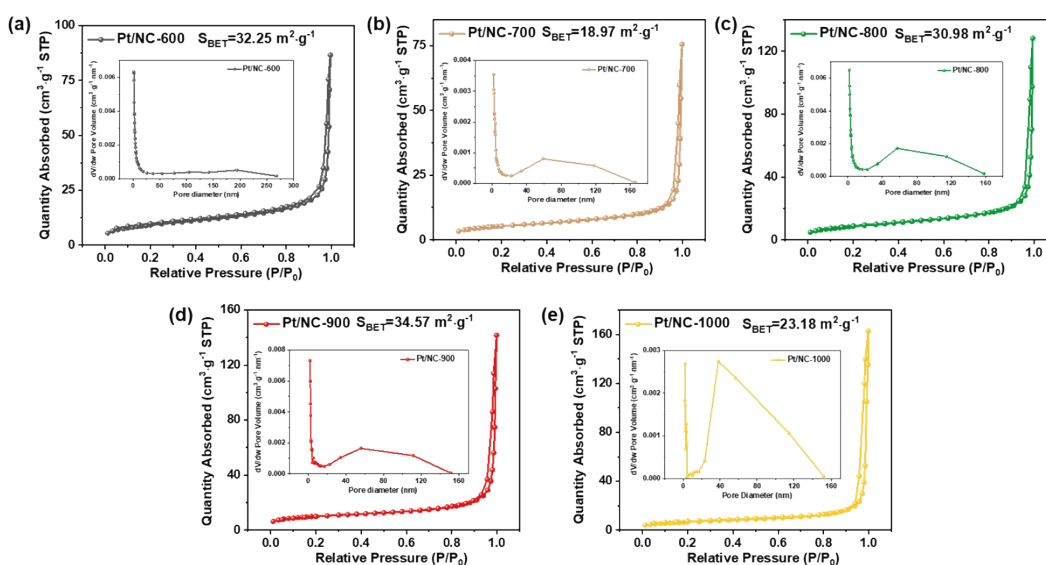


Figure S13. (a-e) N<sub>2</sub> adsorption-desorption isotherm curves and corresponding pore volumes distribution (insets) of the Pt/NC-x (x=600, 700, 800, 900, 1000) electrocatalysts.

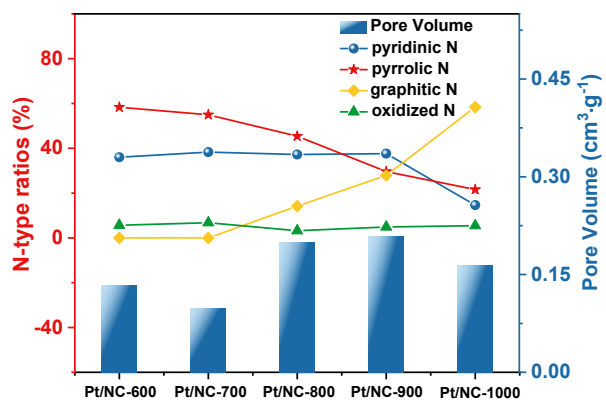


Figure S14. The plot of the pore volume with respect to different N configuration ratios for different Pt/NC-x (x=600, 700, 800, 900, 1000) electrocatalysts.

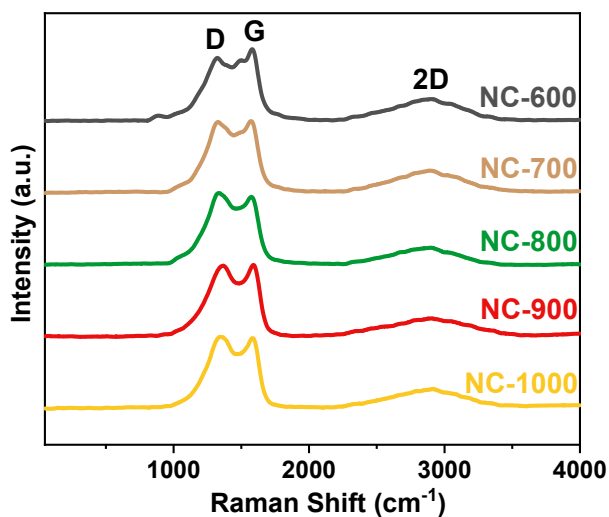


Figure S15. Raman spectra for different NC-x (x=600, 700, 800, 900, 1000 °C) electrocatalysts.

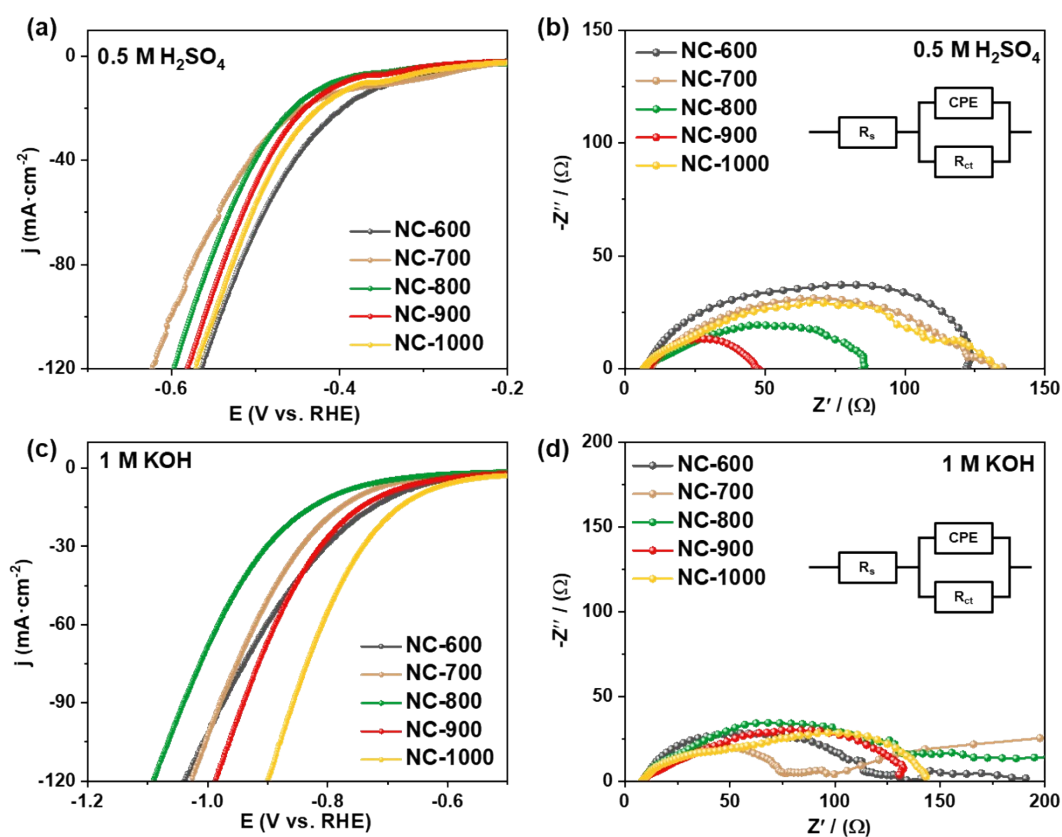


Figure S16. (a) The HER polarization curves, (b) EIS spectra (the inset: the equivalent circuit modeled from the EIS spectra) of NC-x (x=600, 700, 800, 900, 1000) electrocatalysts in 0.5 M H<sub>2</sub>SO<sub>4</sub> electrolyte; (c) The HER polarization curves, (d) EIS spectra (the inset: the equivalent circuit modeled from the EIS spectra) of NC-x (x=600, 700, 800, 900, 1000) electrocatalysts in 1.0 M KOH electrolyte.

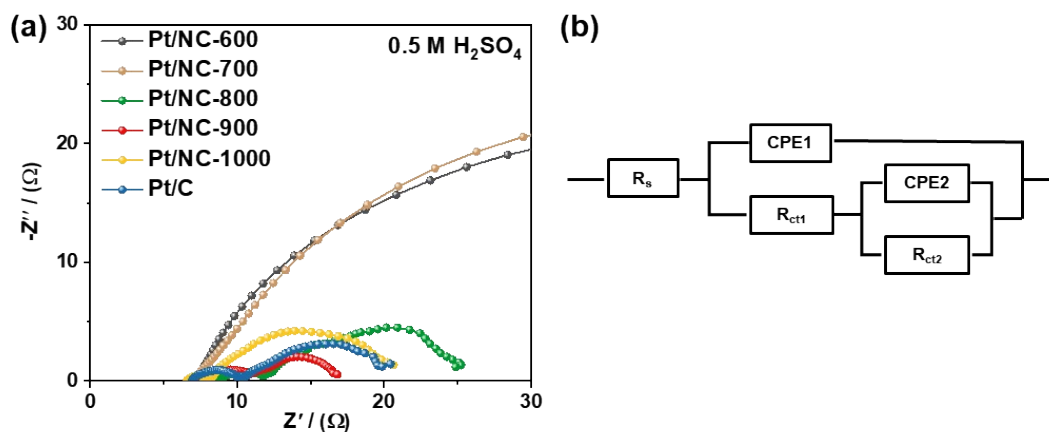


Figure S17. (a) EIS spectra of Pt/NC-x (x=600, 700, 800, 900, 1000) and Pt/C electrocatalysts in 0.5 M H<sub>2</sub>SO<sub>4</sub> electrolyte. (b) The equivalent circuit modeled from the EIS spectra.

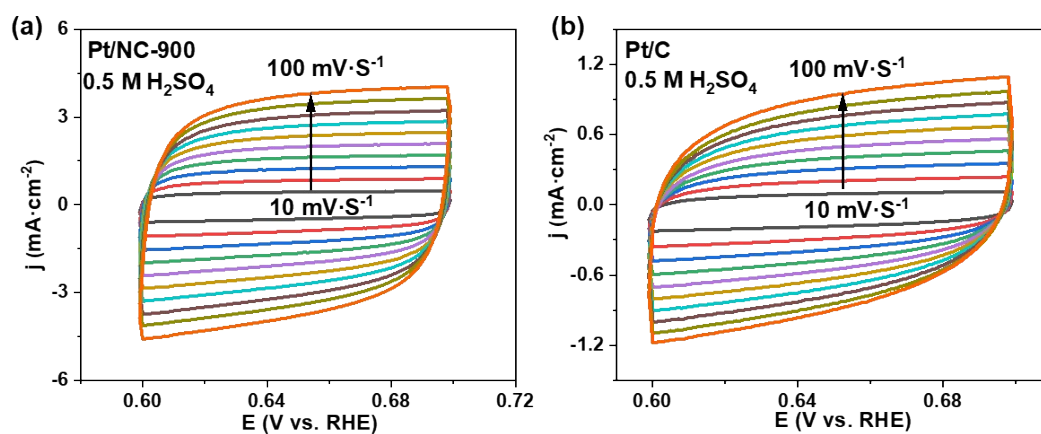


Figure S18. CV curves at different scan rates (10-100 mV s<sup>-1</sup>) of (a) Pt/NC-900; (b) Pt/C in 0.5 M H<sub>2</sub>SO<sub>4</sub>.

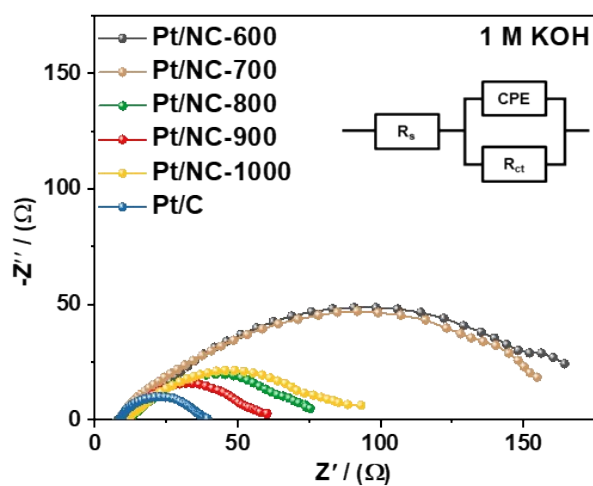


Figure S19. EIS spectra of Pt/NC-x ( $x=600, 700, 800, 900, 1000$ ) and Pt/C electrocatalysts in 1.0 M KOH electrolyte. The inset: the equivalent circuit modeled from the EIS spectra.

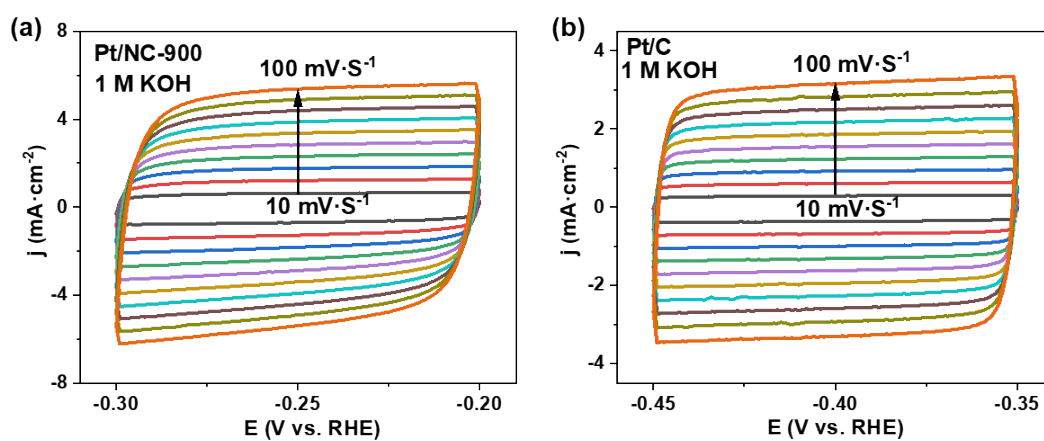


Figure S20. CV curves at different scan rates (10-100  $\text{mV s}^{-1}$ ) of (a) Pt/NC-900; (b) Pt/C in 1.0 M KOH.

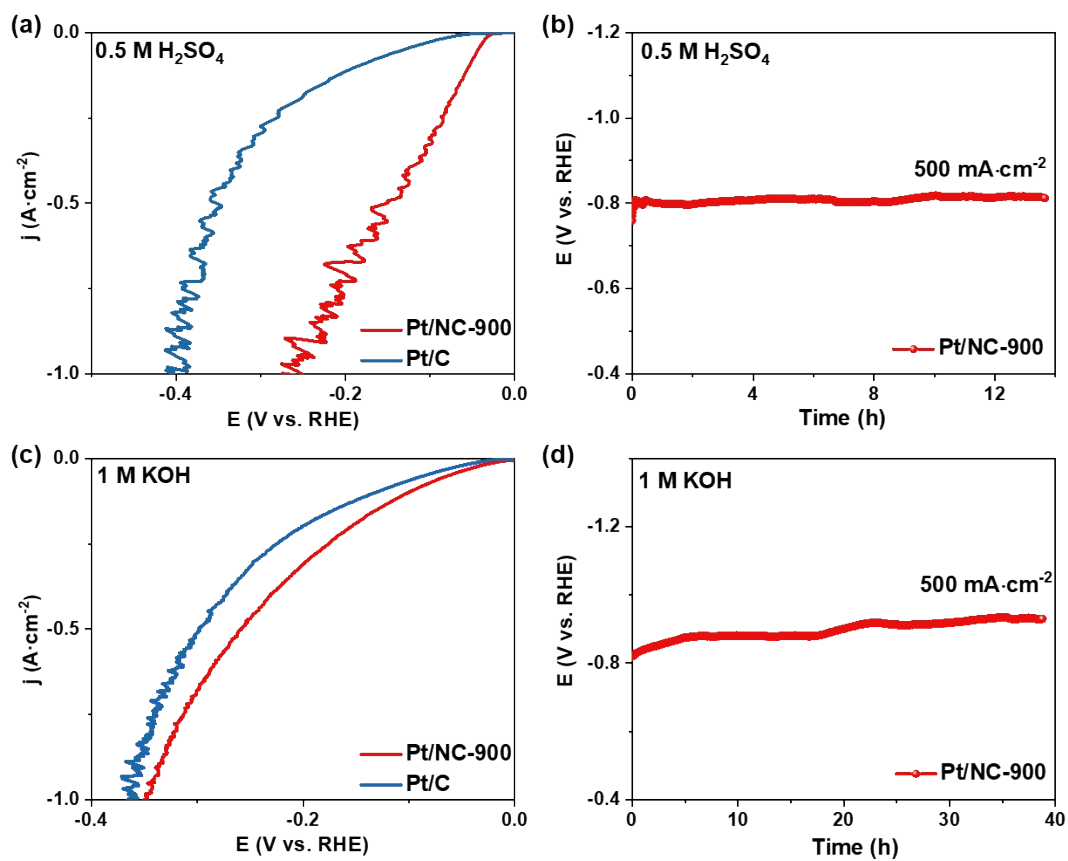


Figure S21. (a) HER polarization curves at high current density and (b) Stability measurement at 500 mA cm<sup>-2</sup> of Pt/NC-900 in 0.5 M H<sub>2</sub>SO<sub>4</sub>; (c) HER polarization curves at high current density and (d) Stability measurement at 500 mA cm<sup>-2</sup> of Pt/NC-900 in 1.0 M KOH.

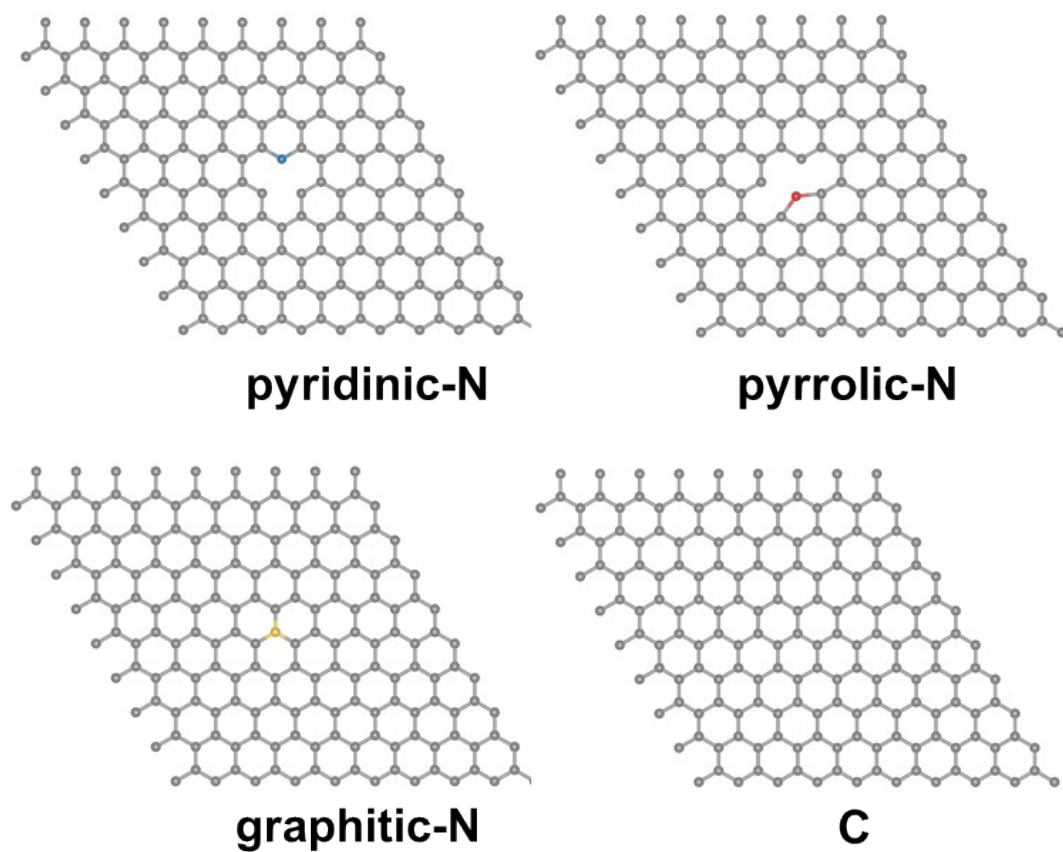


Figure S22. Calculation model structure diagram of pyridinic-N, pyrrolic-N, graphitic-N and C.

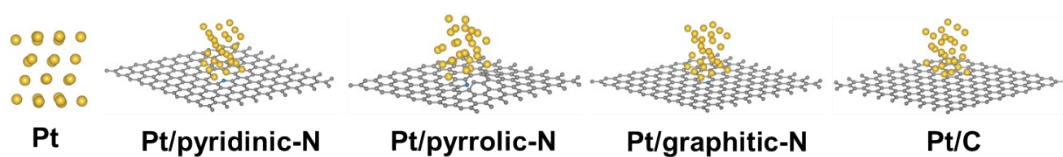


Figure S23. Calculation model structure diagram of Pt, Pt/pyridinic-N, Pt/pyrrolic-N, Pt/graphitic-N and Pt/C electrocatalysts. The gray, blue and golden balls represent the C, N and Pt atoms, respectively.

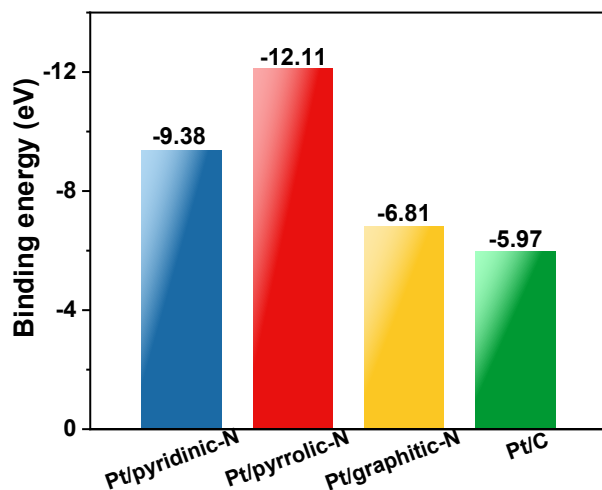


Figure S24. Binding energy for Pt/pyridinic-N, Pt/pyrrolic-N, Pt/graphitic-N and Pt/C.

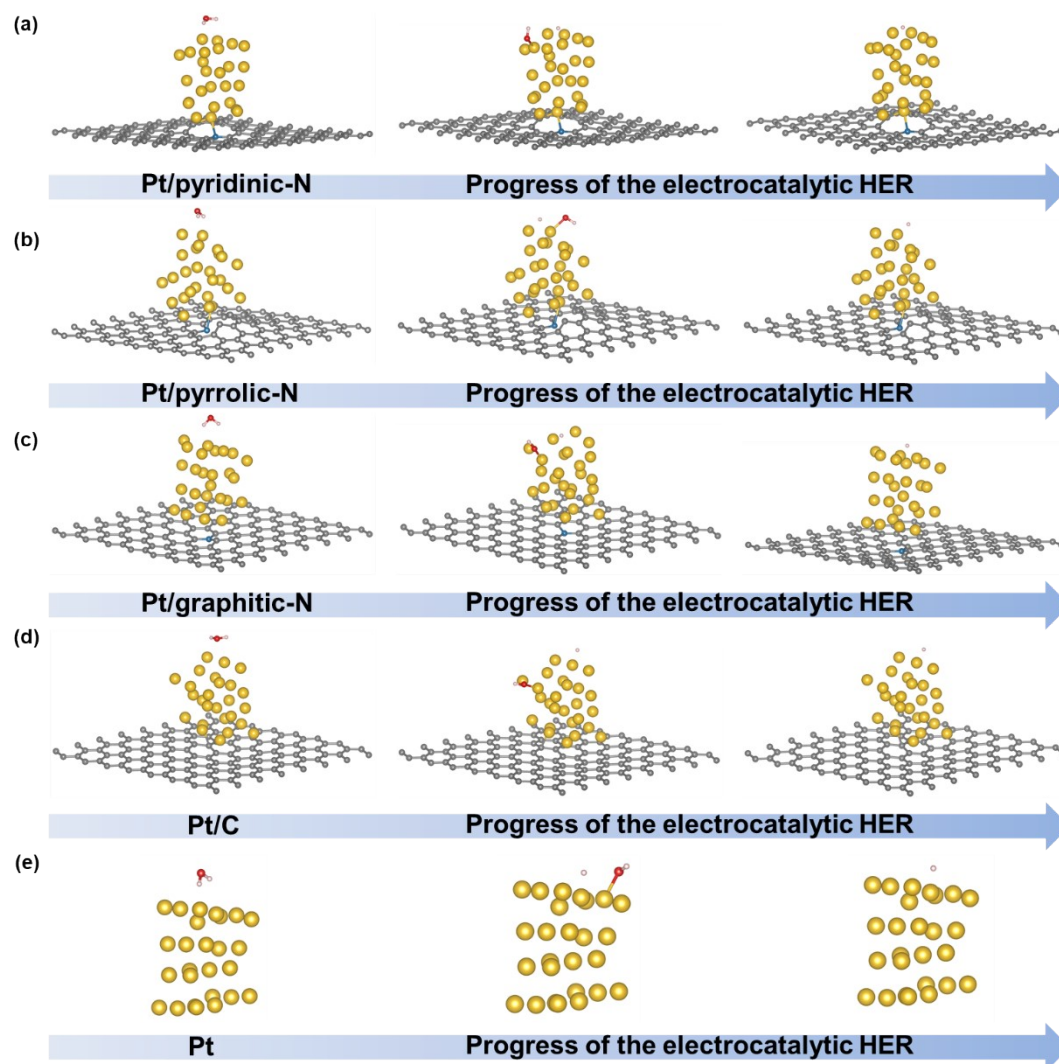


Figure S25. Structural process model diagrams of (a) Pt/pyridinic-N; (b) Pt/pyrrolic-

N; (c) Pt/graphitic-N; (d) Pt/C and (e) Pt for HER.

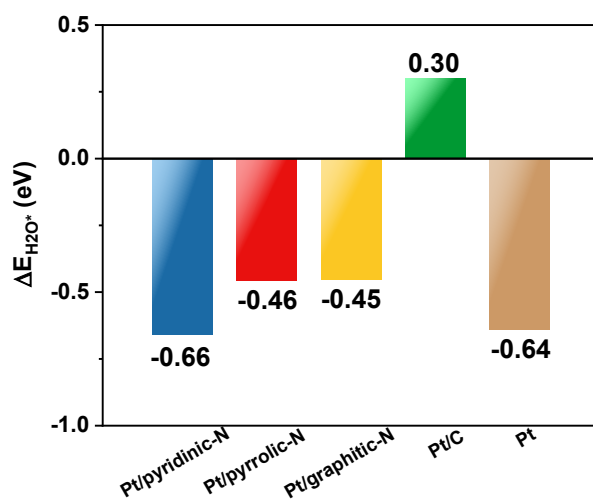


Figure S26. Adsorption energies of  $^*\text{H}_2\text{O}$  ( $\Delta E_{\text{H}_2\text{O}}$ ).

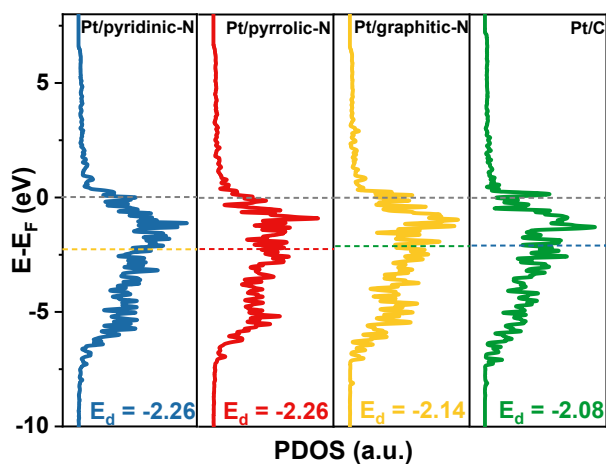


Figure S27. PDOS of Pt 5d for Pt/pyridinic-N, Pt/pyrrolic-N, Pt/graphitic-N, Pt/C and Pt, the d-band centers are labeled  $E_d$ , and the Fermi energy was subtracted to show  $E_F$  at 0.

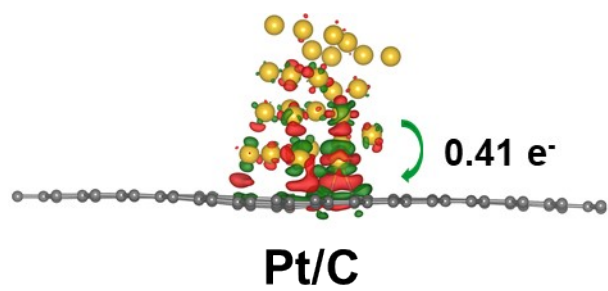


Figure S28. Differential charge density maps of Pt/C. The dark green and red regions represent electron accumulation and depletion, respectively. The iso-surface value is  $0.002 e \text{ \AA}^{-3}$ .

Table S1. The contents of the elements in the different NC-x by the XPS.

Electrocatalysts	NC-600	NC-700	NC-800	NC-900	NC-1000
Zn content / at%	1.06	1.83	1.94	1.04	0.74
N content / at%	27.20	21.97	18.95	15.89	7.05
C content / at%	66.77	71.13	74.42	77.02	87.64
O content / at%	4.97	5.07	4.69	6.01	4.56

Table S2. The weight percentage of Zn elements for NC-x by the ICP-OES.

Electrocatalysts	NC-600	NC-700	NC-800	NC-900	NC-1000
Zn content / wt%	5.123	8.682	8.682	5.688	2.863

Table S3. The relative amount of the different nitrogen species in the different NC-x from the N 1s.

Electrocatalysts	NC-600	NC-700	NC-800	NC-900	NC-1000
Pyridinic N / %	34.98	40.88	43.69	47.05	26.32
Pyrrolic N / %	63.37	53.90	37.93	23.90	19.70
Graphitic N / %	0	0	15.70	26.45	51.77
Oxidized N / %	1.65	5.22	2.68	2.60	2.21

Table S4 The contents of the elements in the different Pt/NC-x by the XPS.

Electrocatalysts	Pt/NC-600	Pt/NC-700	Pt/NC-800	Pt/NC-900	Pt/NC-1000
Pt content / at%	0.96	1.15	1.7	1.28	2.31
Zn content / at%	1.36	1.83	1.65	0.96	0.92
N content / at%	26.55	22.06	18.22	15.16	8.20
C content / at%	65.27	68.33	72.59	75.00	81.93
O content / at%	5.86	6.63	5.85	7.60	6.63

Table S5 The relative amount of the different nitrogen species in the different Pt/NC-x from the N 1s.

Electrocatalysts	Pt/NC-600	Pt/NC-700	Pt/NC-800	Pt/NC-900	Pt/NC-1000
Pyridinic N / %	36.00	38.30	37.21	37.62	14.64
Pyrrolic N / %	58.34	54.94	45.41	29.60	21.55
Graphitic N / %	0	0	14.19	27.90	58.37
Oxidized N / %	5.66	6.76	3.19	4.88	5.44

Table S6 The integral intensity (area) percentage and their ratio of the Pt/NC-x by the Raman.

Electrocatalysts	Pt/NC-600	Pt/NC-700	Pt/NC-800	Pt/NC-900	Pt/NC-1000
I <sub>D</sub>	51.21	50.86	59.60	59.90	59.70
I <sub>G</sub>	22.90	20.42	17.02	16.96	17.41
I <sub>2D</sub>	25.89	28.72	26.38	23.15	22.89
I <sub>D</sub> /I <sub>G</sub>	2.24	2.49	3.50	3.53	3.43

Table S7 The integral intensity (area) percentage and their ratio of the NC-x (x=600, 700, 800, 900, 1000 °C) by the Raman.

Electrocatalysts	NC-600	NC-700	NC-800	NC-900	NC-1000
I <sub>D</sub>	45.67	50.52	58.83	54.87	54.25
I <sub>G</sub>	21.32	19.49	17.58	15.02	17.49
I <sub>2D</sub>	33.01	29.99	23.59	30.11	28.26
I <sub>D</sub> /I <sub>G</sub>	2.14	2.59	3.35	3.65	3.10

Table S8. The weight percentage of Pt and Zn elements for Pt/NC-x by the ICP-OES.

Electrocatalysts	Pt/NC-600	Pt/NC-700	Pt/NC-800	Pt/NC-900	Pt/NC-1000
Zn content / wt%	3.752	7.908	6.681	7.431	2.912
Pt content / wt%	6.616	5.241	10.448	9.108	9.364

Table S9 Mass activities of Pt/NC-900 and Pt/C normalized by mass content of Pt at different overpotentials of 10 mV, 50 mV and 100 mV in acidic.

Electrocatalyst	Mass activity	Mass activity	Mass activity
	(A/mg <sub>Pt</sub> ) @10 mV	(A/mg <sub>Pt</sub> ) @50 mV	(A/mg <sub>Pt</sub> ) @100 mV
Pt/NC-900	0.06	0.61	2.02
Pt/C	0.02	0.17	0.70

Table S10 Mass activities of Pt/NC-900 and Pt/C normalized by mass content of Pt at different overpotentials of 10 mV, 50 mV and 100 mV in alkaline.

Electrocatalyst	Mass activity	Mass activity	Mass activity
	(A/mg <sub>Pt</sub> ) @10 mV	(A/mg <sub>Pt</sub> ) @50 mV	(A/mg <sub>Pt</sub> ) @100 mV
Pt/NC-900	0.11	0.48	1.08
Pt/C	0.03	0.16	0.39

Table S11 The contents of Pt in Pt/NC-900 after 10,000 cycles in 0.5 M H<sub>2</sub>SO<sub>4</sub> and 1 M KOH by the XPS.

Electrocatalysts	Pt content / at%
Pt/NC-900	1.28
Pt/NC-900 after 10,000 cycles in 0.5 M H <sub>2</sub> SO <sub>4</sub>	1.02
Pt/NC-900 after 10,000 cycles in 1 M KOH	0.95

Table S12 The relative amount of the different nitrogen species in the Pt/NC-900 after 10,000 cycles in 0.5 M H<sub>2</sub>SO<sub>4</sub> and 1 M KOH from the N 1s.

Electrocatalysts	Pt/NC-900 after 10,000 cycles in 0.5 M H <sub>2</sub> SO <sub>4</sub>	Pt/NC-900 after 10,000 cycles in 1 M KOH
Pyridinic N / %	18.63	50.39
Pyrrolic N / %	41.89	32.67
Graphitic N / %	39.48	16.94
Oxidized N / %	0	0

Table S13 Comparison of the HER activity of the Pt/NC-900 with other previously reported electrocatalysts in 0.5 M H<sub>2</sub>SO<sub>4</sub> solution.

Catalysts	$\eta_{10}, \eta_{100}$ (mV)	Tafel Slope (mV dec <sup>-1</sup> )	MA@100 mV (A mg <sub>Pt</sub> <sup>-1</sup> )	TOF@100 mV (H <sub>2</sub> s <sup>-1</sup> )	Ref.
Pt/NC-900	33, 96	32.6	2.02	2.04	This work
20wt% Pt/C	39, 110	33.3	0.70	0.70	Commercial
Pd <sub>7</sub> @Pt <sub>3</sub>	33,	23.1	5.65	652.6@150 mV	8
Pt/Ni(OH) <sub>2</sub> /Mo <sub>2</sub> Ti C <sub>2</sub> T <sub>x</sub>	25, 106	26	21.5	9.37@50 mV	9
Pt@CoN <sub>4</sub> -G	21, -	36	1.68@50 mV	1.75@25 mV	10
Pt SAs/MoO <sub>2</sub>	9.3, 81.3	29	69.5@300 mV	-	11
Pt <sub>3</sub> Fe/BNC	38, -	31.3	-	-	12
Pt <sub>3</sub> Fe/NC	89, -	45.6	-	-	
Pt/BNC	65, -	33	-	-	
Pt/C/NF	52, -	104	-	-	13
3D 3h-Pt@Nb <sub>2</sub> CT <sub>x</sub>	33.3, -	29	-	-	14
Pt/NBF-	29, -	24	63.3@50 mV	-	15
ReS <sub>2</sub> /Mo <sub>2</sub> CT <sub>x</sub>					
Pt-TiO <sub>2-x</sub> NSs	36, 180	32.1	0.85@150 mV	-	16
Pt cluster/MXene	34	29		7.9@150 mV	17

Table S14 Comparison of the HER activity of the Pt/NC-900 with other previously reported electrocatalysts in 1 M KOH solution.

Catalysts	$\eta_{10}, \eta_{100}$ (mV)	Tafel Slope (mV dec <sup>-1</sup> )	MA@100 mV (A mg <sub>Pt</sub> <sup>-1</sup> )	TOF@100 mV (H <sub>2</sub> s <sup>-1</sup> )	Ref.
Pt/NC-900	22, 160	54	1.09	1.10	This work
20wt% Pt/C	29, 177	42	0.39	0.40	Commercial
Pd <sub>7</sub> @Pt <sub>3</sub>	49, -	42.7	1.84	220.3@150 mV	8
Pt/Ni(OH) <sub>2</sub> /Mo <sub>2</sub> Ti C <sub>2</sub> T <sub>x</sub>	33, 190	27	17.4	5.9@50 mV	9
Pt@CoN <sub>4</sub> -G	39, -	29	1.15@50 mV	1.31@25 mV	10
Pt SAs/MoO <sub>2</sub>	14, 135	36	41.2@300 mV	-	11
Pt <sub>3</sub> Fe/BNC	24, -	39.4	-	-	12
Pt <sub>3</sub> Fe/NC	77, -	48.3	-	-	
Pt/BNC	50, -	77.6	-	-	
Pt <sub>5A</sub> /α-MoC <sub>1-x</sub> @C	21, -	29	26.65	27.00	18
Pt/C/NF	63, -	82	-	-	13
3D 3h-Pt@Nb <sub>2</sub> CT <sub>x</sub>	61.5, -	58	-	-	14
Pt/NBF- ReS <sub>2</sub> /Mo <sub>2</sub> CT <sub>x</sub>	37, -	36	30.9@50 mV	1.42@150 mV	15
Pt-TiO <sub>2-x</sub> NSs	63, -	50.2	-	-	16
Pt <sub>5A</sub> -Mn <sub>3</sub> O <sub>4</sub>	24, 90	54	0.374@50 mV	10.11@50 mV	19
Pt/MgO	39, -	39			20
Pt/TiB <sub>x</sub> O <sub>y</sub>	210, -	135		33.2@50 mV	21

Table S15 The calculated free energy of the different Reaction intermediates.

	$\Delta G_{\text{H}_2\text{O}^*} / \text{eV}$	$\Delta G_{\text{OH}^*+\text{H}^*} / \text{eV}$	$\Delta G_{\text{H}^*} / \text{eV}$	$\Delta G_{\text{OH}^*} / \text{eV}$
Pt/pyridinic-N	-0.05	0.53	-0.16	-0.68
Pt/pyrrolic-N	0.08	0.59	-0.41	-1.00
Pt/graphitic-N	0.08	0.81	-0.06	-0.87
Pt/C	0.84	1.29	0.55	-0.74
Pt	-0.07	0.62	-0.45	-1.07

## Supplementary References

1. D. L. Wang, H. P. Li, N. Du and W. G. Hou, *Adv. Funct. Mater.*, 2021, **31**, 2009770.
2. P. Hohenberg and W. Kohn, *Physical review*, 1964, **136**, B864.
3. S. Lebegue and O. Eriksson, *Physical Review B*, 2009, **79**, 115409.
4. F. Xiao, Y. Wang, G.-L. Xu, F. Yang, S. Zhu, C.-J. Sun, Y. Cui, Z. Xu, Q. Zhao and J. Jang, *J. Am. Chem. Soc.*, 2022, **144**, 20372-20384.
5. Z. Qiao, C. Wang, C. Li, Y. Zeng, S. Hwang, B. Li, S. Karakalos, J. Park, A. J. Kropf and E. C. Wegener, *Energy Environ. Sci.*, 2021, **14**, 4948-4960.
6. X. Q. Wei, S. J. Song, W. W. Cai, X. Luo, L. Jiao, Q. Fang, X. S. Wang, N. N. Wu, Z. Luo, H. J. Wang, Z. H. Zhu, J. Li, L. R. Zheng, W. L. Gu, W. Y. Song, S. J. Guo and C. Z. Zhu, *Chem*, 2023, **9**, 181-197.
7. Y. Da, Z. Tian, R. Jiang, Y. Liu, X. Lian, S. Xi, Y. Shi, Y. Wang, H. Lu and B. Cui, *Sci. China Mater.*, 2023, **66**, 1389-1397.
8. Y. Liu, N. Yodsinn, T. Li, H. Wu, R. Jia, L. Shi, Z. Lai, S. Namuangruk and L. Huang, *Mater. Horiz.*, 2024, **11**, 1964-1974.
9. S. Liu, Y. Xiang, J. Liu, Z. Du, S. Fang, L. Gao, F. Fu, X. Gao and X. Jian, *Int. J. Hydrogen Energy*, 2024, **63**, 500-509.
10. M. Zhang, H. Li, J. Chen, F. X. Ma, L. Zhen, Z. Wen and C. Y. Xu, *Adv. Funct. Mater.*, 2023, **33**.
11. Y. Qiu, S. Liu, C. Wei, J. Fan, H. Yao, L. Dai, G. Wang, H. Li, B. Su and X. Guo, *Chem. Eng. J.*, 2022, **427**, 131309.
12. Y. Qiao, J. Cui, F. Qian, X. Xue, X. Zhang, H. Zhang, W. Liu, X. Li and Q. Chen, *ACS Appl. Nano Mater.*, 2021, **5**, 318-325.
13. H. Yang, P. Guo, R. Wang, Z. Chen, H. Xu, H. Pan, D. Sun, F. Fang and R. Wu, *Adv. Mater.*, 2022, **34**, e2107548.
14. S. Y. Pang, W. F. Io and J. Hao, *Adv Sci*, 2021, **8**, e2102207.
15. M. Yi, N. Li, B. Lu, L. Li, Z. Zhu and J. Zhang, *Energy Storage Mater.*, 2021, **42**, 418-429.

16. K. M. Naik, E. Higuchi and H. Inoue, *Nanoscale*, 2020, **12**, 11055-11062.
17. Y. Wu, W. Wei, R. Yu, L. Xia, X. Hong, J. Zhu, J. Li, L. Lv, W. Chen, Y. Zhao, L. Zhou and L. Mai, *Adv. Funct. Mater.*, 2022, **32**.
18. W. Wang, Y. Wu, Y. Lin, J. Yao, X. Wu, C. Wu, X. Zuo, Q. Yang, B. Ge, L. Yang, G. Li, S. Chou, W. Li and Y. Jiang, *Adv. Funct. Mater.*, 2021, **32**.
19. J. Wei, K. Xiao, Y. Chen, X. P. Guo, B. Huang and Z. Q. Liu, *Energy Environ. Sci.*, 2022, **15**, 4592-4600.
20. H. Tan, B. Tang, Y. Lu, Q. Ji, L. Lv, H. Duan, N. Li, Y. Wang, S. Feng, Z. Li, C. Wang, F. Hu, Z. Sun and W. Yan, *Nat. Commun.*, 2022, **13**, 2024.
21. X. Cheng, B. Xiao, Y. Chen, Y. Wang, L. Zheng, Y. Lu, H. Li and G. Chen, *ACS Catal.*, 2022, **12**, 5970-5978.